Journal of Molecular Structure 1099 (2015) 154–162

Contents lists available at ScienceDirect

Journal of Molecular Structure

journal homepage: http://www.elsevier.com/locate/molstruc

Syntheses, spectroscopy, X-ray and DFT/TDDFT investigations of Rh(η⁴-cod)-enantiopure aminocarboxylate complexes

Mohammed Enamullah [a, *], Mohammad Khairul Islam [a], Mohammad Abdul Halim [b], Christoph Janiak [c, **]

[a] Department of Chemistry, Jahangirnagar University, Dhaka 1342, Bangladesh
[b] Bangladesh Institute of Computational Chemistry and Biochemistry, 38 Green Road West, Dhaka 1205, Bangladesh
[c] Institute für Anorganische Chemie und Strukturchemie, Heinrich-Heine-Universität, Universitätsstr. 1, D-40225 Düsseldorf, Germany

ARTICLE INFO

Article history:
Received 4 March 2015
Received in revised form
12 June 2015
Accepted 13 June 2015
Available online 17 June 2015

Keywords:
Aminocarboxylic acid
Rh(η⁴-cod)-complex
X-ray structure
Supramolecular chains
DFT/TDDFT calculations

ABSTRACT

The titled Rh(η⁴-cod)-enantiopure aminocarboxylate complexes, [Rh(η⁴-cod) (AA)] {cod = cycloocta-1,5-diene; AA = *L*-prolinato (**1**) and *D*-4-hydroxy-phenylglycinato (**2**)}, are synthesized from the reaction of enantiopure aminocarboxylate with [Rh(η⁴-cod) (acetate)]$_2$. Polarimetric measurements confirm the enantiopurity or very similar enantiomeric excess of the complexes in chloroform. Electronic spectra in different solvents exhibit a negative solvatochromism in the solvents of increasing polarity or acceptor number. DSC analyses show an exothermic peak at 269 °C ($\Delta H = -72.42$ kJ M^{-1}) for **2**, corresponding to an irreversible phase transformation. Cyclic voltammograms reveal a quasi-reversible one electron transfer for [Rh(η⁴-cod) (*L*-prolinate)]/[Rh(η⁴-cod) (*L*-prolinate)]$^+$ couple in acetonitrile. Electronic spectra calculated by TDDFT reveal the bands at relatively lower energy (>230 nm) due to combined d–d, MLCT and LLCT transitions, while the bands at higher energy only for LLCT, which are very similar to the experimental results. X-ray structure demonstrates a distorted square-planar geometry with *N,O*-chelation of the *L*-prolinate ligand to the Rh(η4-cod)-fragment in **1**. The crystal packing is evidenced by charge-assisted intermolecular N–H···O and C–H···O interactions to the non-coordinated carboxylate oxygen atom. Hydrogen bonding leads to the formation of supramolecular chains along the *a* direction of the unit cell. The interchain packing is governed mostly by van-der-Waals forces and reminiscent of a 'herring-bone' packing.

1. Introduction

Syntheses, spectroscopic characterizations and molecular structures of transition metal-complexes with aminocarboxylic acids as ligands are of continued interests [1–5]. Singh et al. first reported the syntheses of dicarbonyl-Rh(I)-aminocarboxylate complexes, [Rh(CO)$_2$(AA)] (AA$^-$ = aminocarboxylato) [1a]. The carbonyl groups can easily be replaced by the soft donor ligands to give [Rh(AA) (L)$_2$] (L = halogen, amines, PPh_3, $AsPh_3$) or [Rh(AA) (L′)] (L′ = 1,2-diamines, 2,2'-bipyridyl, 1,10-phenanthroline) [1b-d]. The cycloocta-1,5-diene (cod) coordinated Rh(I)-aminocarboxylate, [Rh(AA) (η⁴-cod)] was first reported by Marko et al. starting from [Rh(η⁴-cod) (ac)]$_2$, which underwent cod exchange reaction with carbonyl groups to give [Rh(AA) (CO)$_2$] [6]. However, the first structurally elucidated Rh(I)-chiral aminocarboxylate, [Rh(AA) (CO) (PPh_3 or $AsPh_3$)] [7a] and [Rh(L-aziridin-2-carboxylato) (CO)$_2$] [8b] were reported by Beck et al. Stereoselective polymerization of "carbenes" was performed using [Rh(η⁴-cod) (R_1-*L*-proline)] (R_1 = H, benzyl) as effective catalysts [8a]. In addition, Rh(I)-complexes with amino acid based thioamides/hydroxamic acids/hydrazides were used successfully for asymmetric hydrogenation of ketones and ketone derivatives [8b].

We have recently given attention to syntheses, stereochemistry, catalysis and molecular structures determination of Rh(η⁴-cod)-complexes containing the chiral aminocarboxylic acids or amino alcohols as co-ligands starting from the dinuclear [Rh(η⁴-cod) (ac)]$_2$ [9–11]. The most significant observations in our studies are that the achiral *N*-phenylglycinate ligand gives a *racemic* chiral Rh(I)–*N*-phenylglycinate, [Rh(η⁴-cod) (*N*-phenylglycinate)] with

* Corresponding author.
** Corresponding author.
E-mail addresses: enamullah@juniv.edu (M. Enamullah), mahalim@mun.ca (M.A. Halim), janiak@uni-duesseldorf.de (C. Janiak).

http://dx.doi.org/10.1016/j.molstruc.2015.06.040
0022-2860/

the nitrogen atom becoming the stereogenic center upon metal coordination. The crystal structures reveal a case of two-fold spontaneous resolution of a *racemic* mixture into two homochiral helix-enantiomers, namely the (left-handed) $P4_3$- and (right-handed) $P4_1$-helical chain with the *R*- and *S*-*N*-phenylglycinate, respectively [10,11]. The cod ligand in these complexes can easily be replaced with the phosphine ligands (*dppe*/*dppp*/*triphos*) to give the cationic [Rh(*dppe*)$_2$](chiral-aminocarboxylate) or neutral [Rh(*dppp*/*triphos*) (chiral-aminocarboxylate)] complexes [12]. Recently, Rh and Ir complexes have been emerged as attractive luminescent probes, sensors and biotinylation reagents for different biomolecules [13]. The luminescence properties of these complexes are greatly dependent on the nature of solvent and temperature [13d].

The present paper reports the results of syntheses, spectroscopy, DSC, CV, and optical property of [Rh(η^4-cod) (AA)] {AA = *L*-prolinato (**1**) or *D*-4-hydroxy-phenylglycinato (**2**)}. Molecular structure for **1** was determined, and DFT/TDDFT calculations were performed.

2. Experimental

2.1. Materials and physical measurements

All reactions were carried out under an atmosphere of dry nitrogen using Schlenk techniques. Solvents were highly purified, deoxygenated, and distilled prior to their use. FT-IR-spectra were recorded on Nicolet iS10 (Thermo Scientific) spectrometer as KBr discs at ambient temperature. Electronic spectra were obtained with a Shimadzu UV 1800 spectrophotometer in different solvents at 25 °C. Elemental analyses were performed on a VarioEL from Elementaranalysensysteme GmbH. Thermal analyzes was performed on a Shimadzu DSC-60 differential scanning calorimeter (DSC), heating range at 303–553 K and rate at 10 K min^{-1}. Polarimetric measurements were carried with an UniPol L Instrument in $CHCl_3$ or MeOH at 25 °C. An Epsilon™ Instruments (BASi) electrochemical analyzer was used for cyclic voltammetry (CV) experiment containing tetra-N-butyl-ammonium-hexaflorophosphate (TBAP) as supporting electrolyte in acetonitrile at 25 °C. The three-electrode measurement was carried out with a platinum disc working electrode, a platinum wire auxiliary electrode and Ag/AgCl reference electrode. The solution containing **1** and TBAP was deoxygenated for 10 min with nitrogen gas prior to use. ^{1}H NMR spectra were run on a Bruker AC DPX 200 spectrometer operating at 200 MHz (^{1}H) and 50 MHz (^{13}C) at 20 °C. ^{1}H and ^{13}C peaks were calibrated against the DMSO-d_6 solvent signals. Applied Pressure Chemical Ionization (APCI, positive mode) mass spectra were taken on Thermo-Finnigan TSQ 700. Dinuclear [Rh(η^4-cod) (ac)]$_2$ was synthesized from [Rh(η^4-cod)Cl]$_2$ according to our previous literature [9,10]. The enantiopure aminocarboxylic acids, L-proline and *D*-4-hydroxy-phenylglycine were used as received from the Merck.

2.2. General procedure to synthesize the complexes (**1**–**2**)

Two equivalents of L-proline (50 mg, 0.43 mmol) and one equivalent of [Rh(η^4-cod) (acetate)]$_2$ (115 mg, 0.21 mmol) were dissolved in 10 mL of C_6H_6/MeOH (4:1, v/v) and the solution was stirred for 6–8 h at room temperature. The color changed from red-orange to bright-yellow. The solvent was evaporated in *vacuo* at 40 °C. The yellow products were dissolved in 10 mL of C_6H_6/MeOH (4:1, v/v). This solution stirred for another 30 min, and the solvent evaporated again. This procedure was repeated three times, and finally the products were dried in *vacuo* (0.1–0.2 mbar) at 40 °C to give bright yellow compound **1**. The same procedure was followed to synthesize the light ash coloured compound **2** using *D*-4-hydroxy-phenylglycine (HOPhGly). X-ray quality single crystals of **1** were obtained *via* slow evaporation of the solvent from concentrated solution in C_6H_6/MeOH (4:1, v/v) after 2d at room temperature. However, it was not succeeded to grow the single crystal of **2** though several attempts were undertaken.

2.2.1. [(η^4-cod)Rh(L-prolinato-κ^2N,O)] (**1**)

Yield 100 mg (73%). $[\alpha]^{Hg}$: +75.0° (*c* = 0.20 g/100 mL, in $CHCl_3$ at 578 nm and 20 °C). IR (cm^{-1}): 3117s (νNH), 2990w, 2977s, 2931s (νCH), 1620vs (νCO), and 1590sh (δNH). ^{1}H NMR (200 MHz, DMSO-d_6): δ = 1.60 (m, 4H, C*H*$_2$cod$_{exo}$), 1.83 (m, 4H, C*H*$_2$), 2.35 (m, 4H, C*H*$_2$cod$_{endo}$), 2.84 (m, 2H, C*H*$_2$N), 3.55 (m, 1H, C*H*), 4.06 (m, 4H, C*H*cod), and 5.05 (m, 1H, N*H*). $C_{13}H_{20}NO_2Rh$ (325.21): calcd. C 48.01, H 6.20, N 4.31; found C 47.14, H 5.78, N 3.78.

2.2.2. [(η^4-cod)Rh(D-4-hydroxy-phenylglycinato-κ^2N,O)] (**2**)

Yield 120 mg (76%). $[\alpha]^D$: −74.1° (*c* = 0.27 g/100 mL, in MeOH at 589 nm and 20 °C). IR (cm^{-1}): 3226s (νNH$_{asy}$), 3136s (νNH$_{sy}$), 3030w, 3000m, 2950s (νCH), 1625vs (νCO), 1595vs (δNH), and 1580vs (νC = C). ^{1}H NMR (200 MHz, DMSO-d_6): δ = 1.74 (d, *J* = 8.6 Hz, 4H, C*H*$_2$cod$_{exo}$), 2.35 (m, 4H, C*H*$_2$cod$_{endo}$), 3.94 (m, 4H, C*H*cod), 4.07 (d, *J* = 5.6 Hz, 2H, N*H*$_2$), 4.69 (dt, *J* = 6.4, 4.3 Hz, 1H, C*H*), 6.77 (d, *J* = 8.4, 2H, *H*$_m$-Ph), 7.53 (d, *J* = 8.4, 2H, *H*$_o$-Ph), and 9.44 (s, 1H, O*H*). ^{13}C{^{1}H} NMR (50 MHz, DMSO-d_6): δ = 30.6 (*C*H$_2$cod), 61.7 (*C*H), 80.1 (*C*Hcod), 115.2 (*C*$_m$–Ar), 129.2 (*C*$_o$–Ar), 130.5 (*C*–Ar), 157.2 (*C*$_p$-Ar), 181.2 (*C*O$_2^-$) ppm. $C_{16}H_{20}NO_3Rh$ (377.25): calcd. C 50.94, H 5.34, N 3.71; found C 50.97, H 5.36, N 3.62.

2.3. X-ray crystallography

Data Collection: Bruker APEX-II with CCD area-detector, temperature 172(2) K, Mo-Kα radiation (λ = 0.71073 Å), graphite monochromator, ω-scans, data collection and cell refinement with SMART [14], data reduction with SAINT [14], experimental absorption correction with SADABS [15]. *Structure Analysis and Refinement*: The structure was solved by direct methods (SHELXS-97) [16]; refinement was done by full-matrix least squares on F^2 using the SHELXL-97 program suite [16]. All non-hydrogen positions were found and refined with anisotropic temperature factors. The hydrogen atom on nitrogen (-NH) was found and refined with Ueq(H) = 1.2 Ueq(N). Hydrogen atoms on C (CH, CH, and CH$_2$) were calculated with appropriate riding models (AFIX 3, 13, and 23, respectively) and Ueq(H) = 1.2 Ueq(C). Details of the X-ray structure determination and refinement are provided in Table 1. Graphics were drawn with DIAMOND (Version 3.0e) [17].

2.4. Computational method

All calculations were conducted with the Gaussian 09 software package [19]. The initial geometry was generated based on the X-ray structure of compound **1**. Both complexes were optimized and subsequent vibrational frequency calculations were performed using density functional theory employing Becke's (B) [20a] exchange functional combining Lee, Yang, and Parr's (LYP) correlation functional [20b]. Initially 3-21G basis set was employed and then re-optimized by Stuttgart/Dresden (SDD) effective core potential to account relativistic effect of transition metals [20c,d]. Although SDD basis set can be used for all transition metals, it has largely been chosen for Rh complexes [20e-g]. The absence of imaginary frequencies confirmed that the stationary points correspond to minima on the potential energy surface. Molecular orbitals were computed at the same level of theory. For calculating the excited state properties, time-dependent density functional theory (TDDFT) [21a,b] was employed with the B3LYP/SDD level incorporating PCM (Polarization Continuum Model) [21c-e] using acetonitrile as solvent. For TDDFT calculation, 50 excited states were

Table 1
Crystal data and structure refinement for **1**.

Empirical formula	$C_{13}\ H_{20}\ N\ O_2\ Rh$
M (g mol^{-1})	325.21
Crystal size (mm)	0.28 × 0.10 × 0.09
Temperature (K)	172(2)
θ range (°)	2.64 to 30.53
h; k; l range	−14, 15; ±15; ±15
Crystal system	Orthorhombic
Space group	$P2_12_12_1$ (no. 19)
a, b, c (Å)	10.5220(13), 10.6665(14), 11.2163(14)
V (Å^3)	1258.84(30)
Z/D (calc/g cm^{-3})	4/1.716
$F(000)/\mu$ (mm^{-1})	664/1.346
Max/min transmission	0.8850/0.7035
Reflections collected	23198
Independent reflections (R_{int})	3655 (0.0338)
Data/restraints/parameters	3655/0/158
Max./min. $\Delta\rho$ [a]/e Å^{-3}	0.980/−0.993
R_1/wR_2 [$I > 2\sigma(I)$][b]	0.0272/0.0654
R_1/wR_2 (all reflect.)[b]	0.028/0.0662
Goodness-of-fit on F^2[c]	1.076
Absolute structure parameter [18]	−0.03(4)

[a] Largest difference peak and hole.
[b] $R_1 = [\sum(||F_o| - |F_c||)/\sum|F_o|]$; $wR_2 = [\sum[w(F_o^2 - F_c^2)^2]/\sum[w(F_o^2)^2]]^{1/2}$.
[c] Goodness − of − fit = $[\sum[w(F_o^2 - F_c^2)^2]/(n-p)]^{1/2}$.

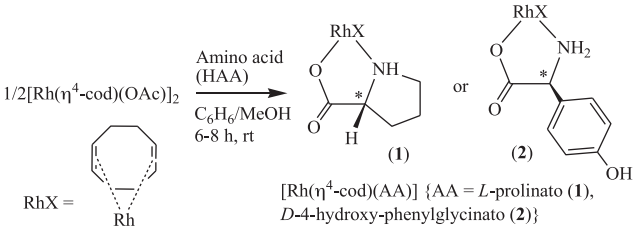

Scheme 1. Synthetic route to the formulation of the compounds **1** and **2**.

Table 2
APCI mass spectral data of compounds **1** and **2**.

1		2	
Ions[a]	[m/z (%)]	Ions[a]	[m/z (%)]
$[M_3-AA]^+$	861 (5)	$[M_3-AA]^+$	965 (7)
$[M_2]^+$	650 (25)	$[M_2]^+$	754 (16)
$[M_2-AA + CO]^+$	564 (5)	$[M_2-AA + C_6H_5]^+$	665 (26)
$[M_2-AA]^+$	536 (16)	$[M_2-AA]^+$	588 (23)
$[M_2-Rh(\eta^4\text{-cod})+H_2]^+$	441 (7)	$[M + C_6H_5+H]^+$	455 (33)
$[M+H]^+$	326 (100)	$[M+H]^+$	378 (100)
$[Rh(\eta^4\text{-cod})]^+$	211 (5)	$[Rh(\eta^4\text{-cod})]^+$	211 (5)

[a] $M/M_2/M_3$ = Mono/di/tri-nuclear species; AA = Aminocarboxylate.

considered (Table S1 and S2).

3. Results and discussion

Enantiopure aminocarboxylate (AA^-) coordinates to the rhodium centre of the dinuclear [Rh(η^4-cod) (acetate)]$_2$ to give the mononuclear [Rh(η^4-cod) (AA)] {AA = *L*-prolinato (**1**) or *D*-4-hydroxy-phenylglycinato (**2**)} in C_6H_6/MeOH (4:1, v/v) (Scheme 1).

3.1. Polarimetry

Polarimetric measurements show the rotation to the right with $[\alpha]^D = +75.0°$ (c = 0.20 g/100 mL) for **1** and to the left with $[\alpha]^D = -74.1°$ (c = 0.27 g/100 mL) for **2**, confirm the enantiopurity or very similar enantiomeric excess of the complexes in chloroform solution [35].

3.2. Mass spectra

Applied Pressure Chemical Ionization (APCI) mass spectra (Figure S1 and Table 2) show the molecular ion peaks for the protonated $[M+H]^+$ species at m/z = 326 (**1**) and 378 (**2**). The spectra further show several ion peaks for the trinuclear $[M_3-AA]^+$, dinuclear $[M_2]^+/[M_2-AA]^+$ and [Rh(η^4-cod)]$^+$ species. The strong intermolecular hydrogen bonding interactions, as evidenced by the X-ray structure determinations for the analogous Rh(η^4-cod)-chiral aminocarboxylate [9–11], lead to the formation of the multinuclear species.

3.3. Solid state and optimized structure

Molecular structure of **1** (Fig. 1) adopts a distorted square-planar geometry with five membered *N*,*O*-chelation of the L-prolinate ligand to the rhodium atom of Rh(η^4-cod)-fragment. The Rh-ligands (*N*,*O*-chelate or cod) bond lengths and angles (Table 3) are comparable to the analogous Rh(η^4-cod)-aminocarboxylate complexes [8a,10,11]. The Rh–NH(prolinate) bond length is little shorter (2.113 Å) than that in Rh–NH(*N*-phenylglycinate) (2.145 Å [10] or 2.151 Å [11]) due to the lower rigidity of the nitrogen atom in the later case. Similarly, the O1–Rh–N angle is slightly larger by 1° in Rh(I)-prolinate (81.9°) compare to that in Rh(I)-*N*-phenylglycinate (80.8°) [10,11].

The experimental structure for **1** and optimized structures for **1** and **2**, calculated at B3LYP/SDD level of theory, are presented in Fig. 1. Selected bond lengths and angles are summarized in Table 3. The calculated and experimental Rh-ligands bond lengths are comparable. Especially the calculated Rh–C1, Rh–C2 O1–C9, O2–C9 and N–C10 bond lengths match closely, while Rh–C5, Rh–C6, C1–C2, and C5–C6 bond lengths are slightly elongated in comparison to those for the experimental values in **1**. However, the calculated and experimental O1–Rh–N, O1–Rh–C1, and O1–Rh–C2 angles show a maximum deviation up to 2°, while

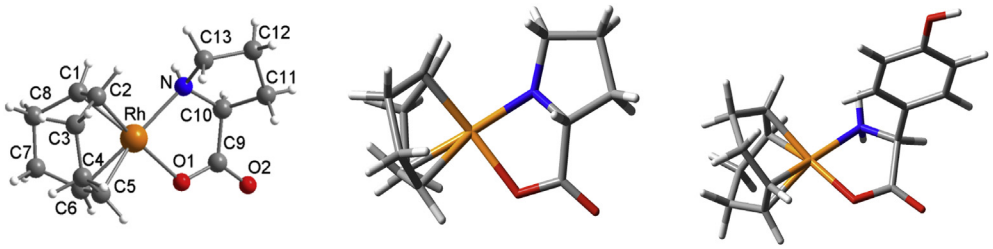

Fig. 1. Molecular structure of **1** (left) and optimized structures of **1** (middle) and **2** (right). Optimized structures are computed at B3LYP/SDD level of theory.

Table 3
Selected bond lengths (Å) and angles (°) in **1** and **2**.

	Exptl. for **1**	Cal. for **1**	Cal. for **2**		Exptl. for **1**	Cal. for **1**	Cal. for **2**
Rh–O1	2.045(2)	2.100	2.050	O1–Rh–N	81.9(9)	78.7	80.3
Rh–N	2.113(2)	2.104	2.155	O1–Rh–C5	94.0(15)	86.6	90.7
Rh–C1	2.082(4)	2.103	2.141	O1–Rh–C6	93.2(14)	104.9	93.8
Rh–C2	2.096(4)	2.111	2.162	N–Rh–C1	96.6(15)	99.7	96.3
Rh–C5	2.113(3)	2.369	2.160	N–Rh–C2	96.5(13)	105.8	100.8
Rh–C6	2.115(3)	2.221	2.174	O1–Rh–C1	158.3(2)	156.3	158.6
O1–C9	1.288(4)	1.339	1.335	O1–Rh–C2	163.7(2)	162.6	162.6
O2–C9	1.231(4)	1.251	1.249				
N–C10	1.497(3)	1.521	1.518				
C9–C10	1.523(4)	1.545	1.568				
C1–C2	1.360(9)	1.467	1.428				
C5–C6	1.342(6)	1.393	1.417				

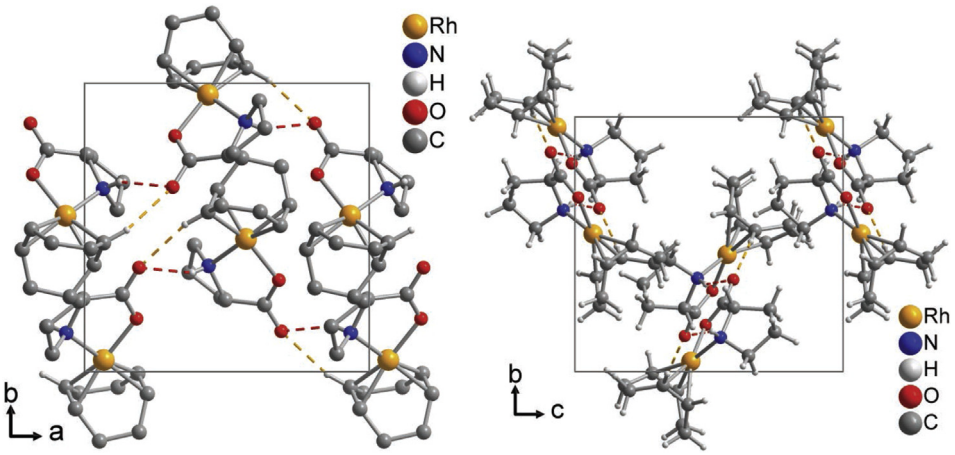

Fig. 2. Section of the packing diagrams of **1** illustrating the intermolecular N–H···O and C–H···O interactions as dashed red and orange lines, respectively; see Table 4 for details. In the left part the H atoms which are not involved in hydrogen bonding have been omitted for clarity. (For interpretation of the references to color in this figure legend, the reader is referred to the web version of this article.)

significant deviations (4–11°) are observed for O1–Rh–C5, O1–Rh–C6, N–Rh–C1, and N–Rh–C2 angles, respectively.

The crystal packing in **1** is organized by charge-assisted [22] intermolecular N–H···O and C–H···O interactions to the non-coordinated carboxylate oxygen atom (Fig. 2, Table 4). The C–H···O interaction [22h] originates from the cod ligand. In "charge-assisted" hydrogen bonds, the hydrogen bond donor and/or acceptor carry positive and/or negative ionic charges, respectively. The enhancement of hydrogen bond strength, which may be linked to robustness by ionic charge, has long been recognized and some of the strongest hydrogen bonds are "charge-assisted" [22]. The hydrogen bonding in **1** leads to the formation of supramolecular chains which run along the *a* direction of the unit cell (Fig. 3). The interchain packing is then governed mostly by van-der-Waals forces and reminiscent of a 'herring-bone' packing (Fig. 3).

3.4. Infrared spectra

Experimental FT-IR (Figure S2) show a very strong carbonyl (νCO) band at 1620 (**1**) and 1625 (**2**) cm^{-1}. One strong broad νNH stretching band is found at 3117 cm^{-1} in **1**, while two strong broad νNH_2 stretching bands are found at 3226 and 3136 cm^{-1} (asymmetric and symmetric) in **2** [6–12]. Both compounds show weak bands at the range of 3050–2930 cm^{-1} for νCH. Computed IR spectra (Figure S3) show the unscaled carbonyl band at 1654 cm^{-1}. The B3LYP functional can reproduce the experimental vibrational

Table 4
Hydrogen bonds in the crystal structure of 1.[a]

D-H···A	D-H (Å)	H···A (Å)	D···A (Å)	D-H···A (°)	Symmetry
N1–H1n … O2	0.75(5)	2.28(5)	2.980(3)	155(5)	1/2 + x,3/2-y,2-z
C1–H1 … O2	0.99	2.45	3.409(5)	164	1/2 + x,3/2-y,2-z

[a] Bond lengths and angles between found and refined atoms are given with standard deviations.

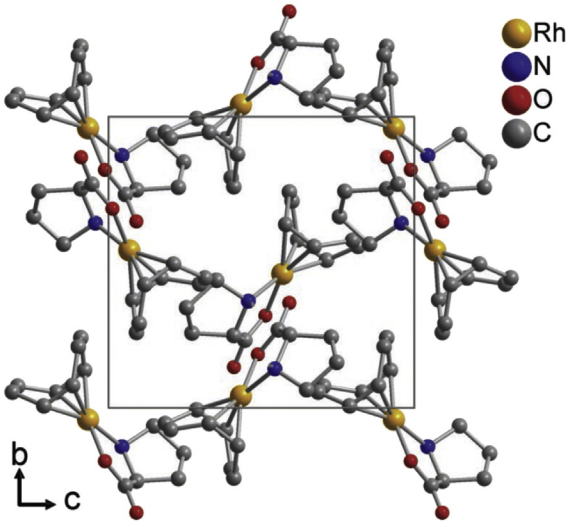

Fig. 3. Intermolecular packing viewed along *a* to illustrate a 'herring-bone' type packing governed by van-der-Waals interactions. Hydrogen atoms are not shown for clarity.

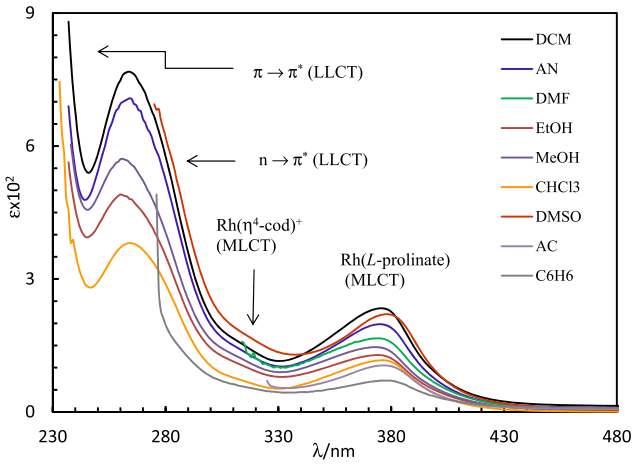

Fig. 4. Electronic spectra of compound **1** in different solvents at 25 °C.

frequency; however, scaling factors (0.9613–0.9688) are required for different basis sets [23]. Since the SDD basis set has greater performance on reproducing the experimental vibrational frequencies, scaling factor of 0.9800 can provide very comparative results. Applying 0.9800 as scaling factor, the vibrational frequency for carbonyl band shifts the to 1621 cm^{-1}, almost same as the experimental values. Thus, the computed νNH (scaled) appears at 3337 cm^{-1} in **1**, while $\nu NH_{asy}/\nu NH_{sy}$ (scaled) appears at 3478/3383 cm^{-1} in **2**.

3.5. Electronic spectra

Electronic spectra of **1** and **2** in different solvents (Fig. 4, Figure S4 and Table 5) feature a very strong band below 245 nm (λ_{max} = 225–228 nm for **2**), and a strong broad band at 245–300 nm (λ_{max} = 260–265 nm for **1** and 258–262 nm for **2**), associated with the intra-ligand $\pi \rightarrow \pi^*$ and $n \rightarrow \pi^*$ transitions (LLCT), respectively [9–12]. The spectra further show a weak shoulder at 300–330 nm and a medium broad band at 330–450 nm (λ_{max} = 373–378 nm for **1** and 370–373 nm for **2**) (Table 5). The shoulder and band are assigned to the metal-to-ligand charge transfer (MLCT) transitions based on the formation of Rh(η^4-cod)$^+$ and Rh(aminocarboxylate) species in [Rh(η^4-cod)(aminocarboxylate)] [9–12]. Indeed, these two MLCT bands are shown separately with λ_{max} at 316, 371 nm in acetonitrile, and at 351, 390 nm in DMSO for **2** (Figure S4). For comparison study, the spectrum of *D*-4-hydroxy-phenylglycine (free ligand) is shown in Figure S4, which shows two LLCT bands: a very strong band at <250 nm and a strong broad band at 250–290 nm (λ_{max} = 276 nm), while no further bands above 290 nm like those in compound **2**.

TDDFT spectra (Fig. 5), calculated at the B3LYP/SDD level of theory in acetonitrile, show several bands/shoulders similar to the experimental spectra (Fig. 4, Figure S4), and their assignments are listed in Table 6. The bands at relatively lower energy are mainly due to the combined d–d and MLCT (or d–d, MLCT, and LLCT) transitions, while bands at higher energy (<230 nm) for LLCT transitions. The excited states related to d–d, MLCT and LLCT transitions overlapped with each other and difficult to interpret as the respective excited states are quite close in energy [13e,23c,24,25]. Although the d–d transitions are not allowed, however, distortion from square-planar geometry and coupling of the σ-type ligand orbitals with the metal d-orbitals exhibit the d–d excitation [23,24]. Thus, only the selected and simplified assignments related to the experimental data are discussed here. The combined d–d and MLCT transitions appear with absorption maxima at 364 (**1**) or 365 nm (**2**) with a high molecular orbital (MO) contribution of 75% (HOMO to LUMO+1 for **1**) and 91% (HOMO to LUMO for **2**), which are very close to the experimental values {375 (**1**) or 371 nm (**2**)}. There are also several TDDFT bands which are in good agreement with the experimental bands. The HOMOs and LUMOs for the compounds are presented in Fig. 6.

3.6. Solvatochromism

Electronic spectra at different time intervals reveal that compound **1** dissociates up to *ca.* 2% within 2 h of dissolution (*ca.* 15%

Table 5
Electronic spectral data of compounds **1** and **2** in different solvents at 25 °C.

Solvent[b]	$\pi \rightarrow \pi^*$: LLCT ($\lambda_{max}/\varepsilon_{max}$)[c]	$n \rightarrow \pi^*$: LLCT ($\lambda_{max}/\varepsilon_{max}$)[c]	Rh(η^4-cod)$^+$: MLCT ($\lambda_{max}/\varepsilon_{max}$)[c]	Rh(AA): MLCT[a] ($\lambda_{max}/\varepsilon_{max}$)[c]
1				
MeOH (0.43)	<245	245-300 (261/5710)	300-330 sh	330-430 (373/1463)
EtOH (0.49)	<245	245-300 (260/4909)	300-330 sh	330-430 (374/1285)
AN (0.43)	<245	245-300 (264/7076)	300-330 sh	330-430 (375/1981)
AC (0.42)	–	–	–	330-430 (377/1052)
DMF (0.51)	–	–	300-330 sh	330-430 (374/1661)
C_6H_6 (0.10)	<280	280-300 sh	300-330 sh	330-430 (378/707)
DCM (0.33)	<245	245-300 (264/7677)	300-330 sh	330-430 (376/2342)
$CHCl_3$ (0.28)	<245	245-300 (265/3809)	300-330 sh	330-430 (376/1167)
DMSO (0.43)	–	<280	300-330 sh	330-430 (377/2202)
MeOH (0.27)[d]	<245	240-300 sh	300-330 sh	320-430 (350/826)
2				
MeOH (0.16)	<245 (228/16580)	250-300 (262/4623, 272sh)	300-330 sh	330-430 (370/1148)
EtOH (0.18)	<245 (225/17667)	250-300 (261/5136, 272sh)	300-330 sh	330-430 (370/1316)
AN (0.08)	<245 (227/24720)	250-300 (258/5013, 272 sh)	300-330 (316/967)	330-430 (371/1870)
AC (0.09)	–	–	300-330 sh	330-430 (373/3020)
DMF (0.18)	–	–	300-330 sh	330-430 (371/2808)
DMSO (0.15)	<260	260-325 (276/7870, 280sh)	330-370 (351/1894)	370-430 (390/1254)
HOPhGly (0.08)[e]	<250	250-290 (276/6481, 280sh)	–	–

[a] AA = *L*-prolinate for **1** and *D*-4-hydroxy-phenylglycinate for **2**.
[b] Concentration in parentheses in $mM \cdot L^{-1}$.
[c] λ_{max} in nm, ε_{max} in $L \cdot mM^{-1} \cdot dm^{-3}$.
[d] Addition of excess acetic acid (30%, v/v) into methanolic solution of **1**, until no further changes of spectra.
[e] HOPhGly = *D*-4-hydroxy-phenylglycine in MeOH.

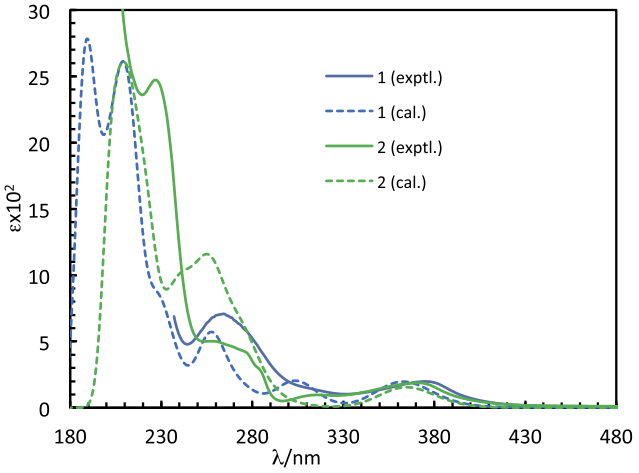

Fig. 5. Electronic spectra (experimental and calculated) of **1** and **2**, calculated at B3LYP/SDD level of theory, in acetonitrile (Gaussian band shape with 0.16 eV exponential half-width).

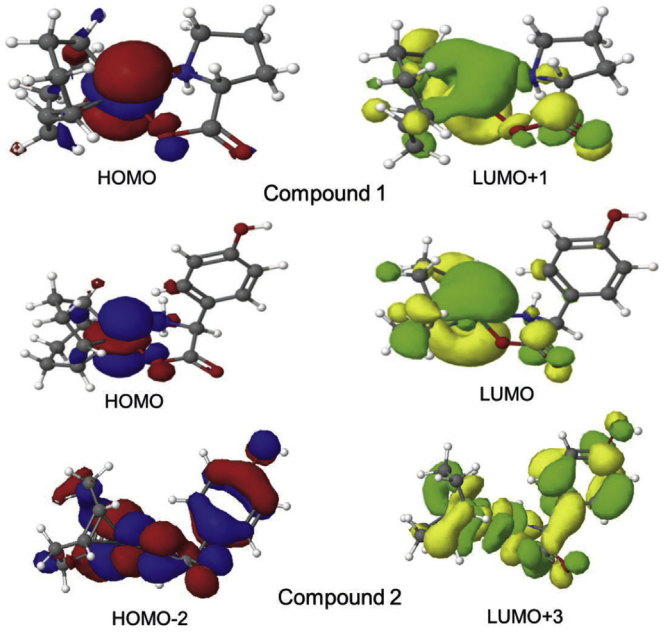

Fig. 6. The HOMOs and LUMOs (isosurface 0.02) for **1** and **2**, calculated at B3LYP/SDD level of theory, in acetonitrile.

within 12 h) in chloroform or methanol. In strong coordinating solvents like tetrahydrofurane or cyclohexanone, both compounds are fully dissociated within 10–15 min of dissolution. In these solvents the MLCT bands completely disappear with intensifying the LLCT band with time. However, to study exclusively the solvatochromism, spectra are taken within 5 min of compound dissolution (when no dissociation occurs) in nine different solvents (Fig. 4, Figure S4, Table 5). Both absorption maxima (λ_{max}) and intensities (ε_{max}) are changed with the polarity (μ/Debye) or Gutmann's acceptor number (AN) [26a] of the solvents. The results show a negative trend of solvatochromism with shifting λ_{max} to the higher energies (blue shift) in the solvents of increasing polarity (μ/Debye) (Fig. 7, left) or acceptor number (AN) (Fig. 7, right) [26–29].

3.7. Hydrolysis of **1** in acetic acid solution

Successive additions of aqueous acetic acid (30%, v/v) into methanolic solution of [Rh(η^4-cod) (*L*-prolinate)] (**1**) result in hydrolysis and formation of the hydrated $[Rh(\eta^4\text{-cod})\ (H_2O)_2]^+$, accompany a change in the spectra (Fig. 8, Table 5) [30]. Thus, MLCT band with λ_{max} at 373 nm due to Rh(*L*-prolinate) disappears with the formation of a new band with λ_{max} at 350 nm for $Rh(H_2O)^+$ in $[Rh(\eta^4\text{-cod})\ (H_2O)]^+$. Here, n → π* (LLCT) band also disappears/shifts, while the shoulder for $Rh(\eta^4\text{-cod})^+$ remains almost unchanged. The related $[CpRh(bpy)\ (H_2O)]^{2+}$ shows the absorption band with λ_{max} at 358 nm [30a]. Solid state structures of $[Rh(\eta^4\text{-cod})\ (H_2O)_2](CF_3SO_3)$ [30b] and $[Rh(\eta^4\text{-cod})\ (L)\ (H_2O)](BF_4)$ {L = 1-(2-methoxyethoxymethyl)-3,5-dimethylpyrazole} [30c] have been reported. In fact, the presence of several isosbestic points at 407, 355, 320 and 253 nm indicates the existing equilibria among different ionic species in solution. Electronic spectrum of the precursor, $[Rh(\eta^4\text{-cod})\ (ac)]_2$ shows two strong bands with λ_{max} at 355 and 421 nm [9,12], which rules out the formation of any $Rh(\eta^4$-

Table 6
Selected excitation properties of compounds **1** and **2** calculated at B3LYP/SDD level of theory in acetonitrile.

Wavelength (nm)[a]	Oscillator strength	Electronic transition (MO contribution, %)[b]	Assignments[c]
Compound 1			
448	0.0006	H→L (81%), H→L+1 (15%)	d–d, MLCT
387	0.0016	H-1→L (64%), H-1→L+1 (11%)	d–d, MLCT
364 (375)	0.0213	H→L+1 (75%), H→L (13%)	d–d, MLCT
348	0.0029	H-2→L (33%), H-1→L (11%) H-3→L (19%), H-2→L+1 (16%)	d–d, MLCT, LLCT
304 (ca. 310sh)	0.0156	H-1→L+1 (61%), H→L+2 (12%)	d–d, MLCT, LLCT
258 (264)	0.0313	H-1→L+2 (38%), H-3→L+1 (15%) H-2→L+1 (17%)	d–d, MLCT, LLCT
207	0.0935	H-2→L+5 (48%), H-2→L+6 (15%)	LLCT
190	01240	H-4→L+4 (23%), H-3→L+7 (10%) H-8→L(15%)	LLCT
Compound 2			
391	0.0005	H→L+3 (46%), H→L+2 (36%) H→L+1 (14%)	d–d, MLCT
365 (371)	0.0178	H→L (91%)	d–d, MLCT
344	0.0014	H-1→L+3 (28%), H-1→L+2 (19%) H-3→L+3 (12%)	d–d, MLCT, LLCT
310 (316)	0.0011	H-1→L (24%), H-2→L+3 (19%), H-2→L+2(16%)	d–d, MLCT, LLCT
274 (272sh)	0.0422	H-2→L (45%), H→L+4 (35%)	d–d, MLCT, LLCT
260 (258)	0.0402	H-3→L(26%), H-4→L(18%), H→L+9(19%)	d–d, MLCT, LLCT
223 (227)	0.0757	H-5→L(22%), H-4→L+3(20%)	LLCT
211	0.0765	H-7→L(29%), H-5→L+2(24%)	LLCT

[a] Experimental values are in parentheses.
[b] H for HOMO and L for LUMO molecular orbital.
[c] MLCT = metal-to-ligand charge transfer, LLCT = intra-ligand charge transfer; d–d = metal centered d–d transitions.

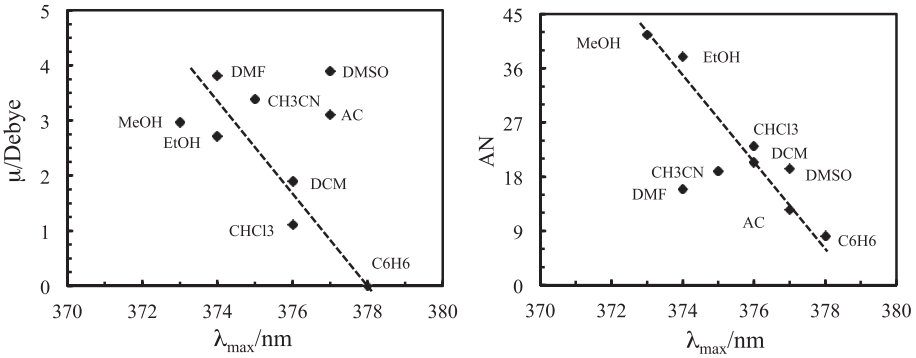

Fig. 7. Changes of absorption maxima (λ_{max}) with increasing polarity (μ) (left) or acceptor number (AN) (right) of the solvents for **1** at 25 °C.

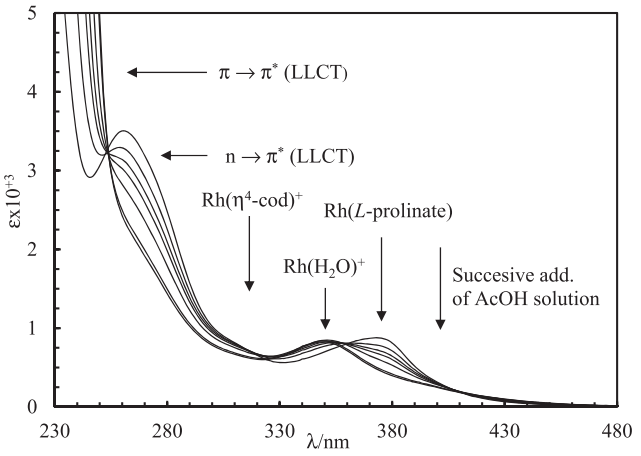

Fig. 8. Changes of electronic spectra with successive additions of acetic acid solution (30%, v/v) into methanolic solution of **1** at 25 °C.

cod)-acetate species in aqueous acetic acid solution.

3.8. NMR spectra

In ^{1}H NMR spectra (Fig. 9), the rhodium-coordinated 1,5-cyclooctadiene ligand shows two multiplets at δ 1.60 (**1**)/1.74 (**2**) and 2.35 ppm (**1** or **2**) for the exo- and endo-methylene protons (CH_2cod), respectively, while one multiplet at δ 4.06 (**1**)/3.94 ppm (**2**) for the methine protons (*CH*cod) [9–11,31–34]. The methylene (CH_2/CH_2N), methine (*CH*), and amino (N*H*) protons on the coordinated L-prolinate ligand are shown as multiplets at δ 1.83/2.84, 3.55, and 5.05 ppm, respectively in **1**. Similarly, the methine (*CH*), amine (NH_2), and phenolic (O*H*) protons on the coordinated *D*-4-hydroxy-phenylglycinate ligand are found as a doublet of triplet at δ 4.69 ppm (J = 6.4, 4.3 Hz), doublet at δ 4.07 ppm (J = 5.6 Hz), and singlet at δ 9.44 ppm, respectively in **2** (Fig. 9). The *ortho*- and *meta*-aromatic protons show two doublets at δ 7.53 and 6.77 ppm (J = 8.4 Hz), respectively. In ^{13}C NMR spectrum, the coordinated 1,5-cyclooctadiene shows a singlet at δ 30.6 ppm for CH_2cod and a weak broad peak at *ca.* δ 80.1 ppm for *CH*cod in **2**. The methine (*CH*) and carboxylate (CO_2^-) carbons on *D*-4-hydroxy-phenylglycinate ligand are shown as singlet at δ 61.7 and 181.2 ppm, respectively. Different singlets for aromatic carbons are found at δ 115.2 (C_m), 129.2 (C_o), 130.5 (*C*–Ar) and 157.2 (C_p) ppm, respectively in **2**.

3.9. Thermally induced structural phase transformation

It has been well documented that the transition metal complexes containing *N*,*O*-chelate ligands exhibit thermally induced structural phase transformation from low temperature crystalline phase (distorted tetrahedral/square planar) to high temperature isotropic liquid phase (regular tetrahedral/square planar). The differential scanning calorimetry (DSC) curve of heating (Fig. 10) shows an exothermic peak at 268.6 °C (ΔH = −72.42 kJ M^{-1}), corresponds to a phase transformation from crystalline to isotropic liquid phase for **2**, as observed for related transition metal *N*,*O*-chelate complexes [24,25,27a,28]. The absence of any peak on the cooling curve indicates an irreversible phase transformation. However, the DSC curve of heating shows a broad endothermic peak (Fig. 10) which corresponds to an irreversible decomposition of **1** [35].

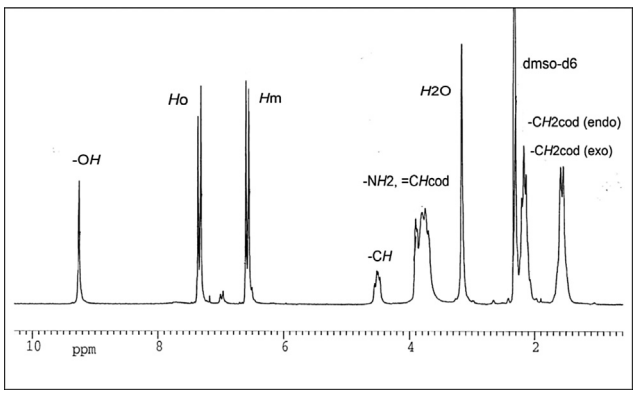

Fig. 9. ^{1}H NMR spectrum of compound **2** in DMSO-d_6 at 20 °C.

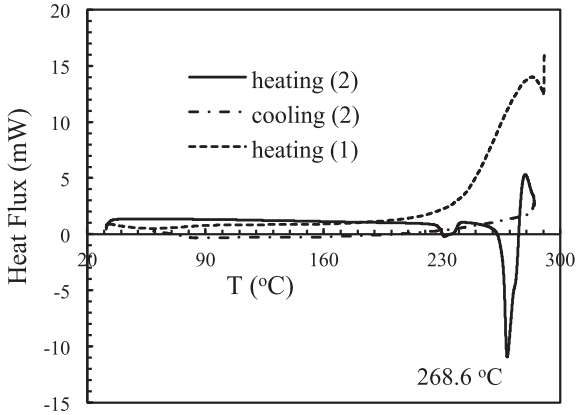

Fig. 10. Differential scanning calorimetry (DSC) curves for compounds **1** and **2**.

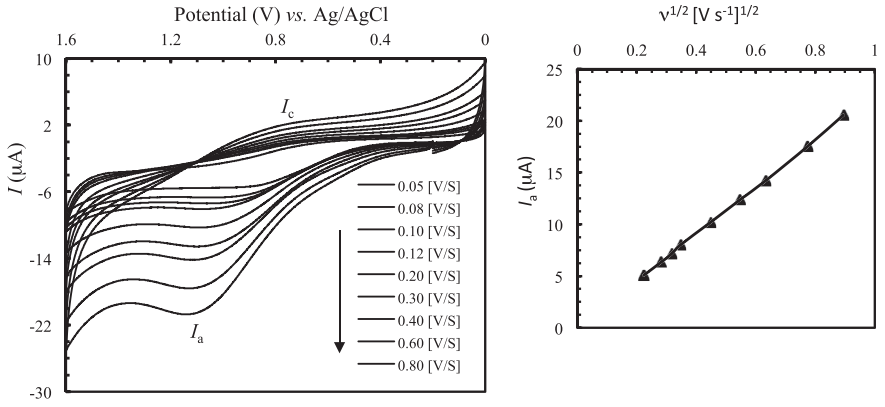

Fig. 11. Cyclic voltammograms (left) and changes of anodic peak current (right) of **1** (0.5 mmol dm^{-3}) at different scan rates in acetonitrile at 25 °C; TBAP (0.1 mol dm^{-3}).

3.10. Cyclic voltammetry

Cyclic voltammogram of **1** was recorded starting from 0.2 to 1.60 V then to 0.2 V (*versus* Ag/AgCl), using different switching potentials at varying scan rates in acetonitrile (Fig. 11, left). The oxidative response shows an anodic wave with E_{pa} = 0.86 V (I_a = −5.21 μA) for [Rh(η⁴-cod) (AA)]/[Rh(η⁴-cod) (AA)]$^+$ (AA = *L*-prolinato) couple at scan rate of 0.05 Vs^{-1}. The wave becomes more intense and shifts to higher potential with increasing scan rate at 0.80 Vs^{-1} (E_{pa} = 1.10 V, I_a = −20.55 μA). The corresponding reductive response shows a very poor cathodic wave, which becomes significant at higher scan rate of 0.80 Vs^{-1} (E_{pc} = 0.82 V, I_c = 1.64 μA). The cationic [Rh(η⁴-cod) (AA)]$^+$, produced on the anodic scan, is very unstable and undergoes rapid chemical transformation, results in a poor cathodic wave for Rh(II)/Rh(I). Analyses of voltammograms demonstrate that both the anodic peak current (I_a) and potential separation (ΔE_p) increase at faster scan rates (Fig. 11, right). The results support a quasi-reversible one electron transfer process for Rh(I)/Rh(II) couple as found for the related square-planar Rh(I)-complexes [36].

4. Conclusion

Enantiopure aminocarboxylate coordinates to the dinuclear [Rh(η⁴-cod) (ac)]$_2$ to give mononuclear [Rh(η⁴-cod) (AA)] (**1**—**2**) *via* anion exchange reaction. X-ray structure demonstrates a distorted square-planar geometry with *N*,*O*-chelation of the *L*-prolinate ligand to Rh(η⁴-cod)-fragment in **1**. The crystal packing is originated from charge-assisted intermolecular N—H···O and C—H···O interactions to the non-coordinated carboxylate oxygen atom. The hydrogen bonding leads to the formation of supramolecular chains along the *a* direction of the unit cell. DFT/TDDFT calculations on vibrational and electronic spectra reveal several bands which are very similar to the experimental results. Electronic spectra in different solvents show a negative solvatochromism in the solvents of increasing polarity or acceptor number. DSC analysis corresponds to an irreversible phase transformation from crystalline to isotropic liquid phase for **2**. CV results demonstrate a quasi-reversible one electron transfer for Rh(I)/Rh(II) couple in acetonitrile. The present results explore the photophysical properties of Rh(I)-aminocarboxylate complexes which will be useful in analyzing their uses as catalysts (for asymmetric hydrogenation, polymerization and C—H bond activation reactions) and biomolecules (for luminescent probes, sensors and biotinylation reagents).

Acknowledgments

We acknowledge the "Wazed Miah Science Research Centre" at Jahangirnagar University, Dhaka, Bangladesh for obtaining CV and elemental data. Our sincere thank to Professor K.S. Hagen, Department of Chemistry, Emory University, Atlanta for X-ray analysis of **1**. For allocating computational resource and time, we are also thankful to Professor Raymond Poirier, Department of Chemistry, Memorial University, Canada, and the Atlantic Computational Excellence Network (ACEnet).

Appendix A. Supplementary data

Supplementary data related to this article can be found at http://dx.doi.org/10.1016/j.molstruc.2015.06.040.

References

[1] (a) D. Dowerah, M.M. Singh, Trans. Met. Chem. 1 (1976) 294;
(b) D. Dowerah, M.M. Singh, J. Indian Chem. Soc. LVII 368 (1980);
(c) D. Dowerah, M.M. Singh, J. Chem. Res. (S) (1979) 38;
(d) D. Dowerah, M.M. Singh, J. Chem. Res. M. (1979) 0255.
[2] (a) K. Severin, K. Sünkel, W. Beck, Chem. Ber. 127 (1994) 615;
(b) K. Severin, W. Beck, Z. Naturforsch. B 50 (1995) 275;
(c) J. Cai, X. Hu, X. Feng, W. Shao, L. Ji, I. Bernal, Eur. J. Inorg. Chem. (2000) 2199;
(d) K. Prout, S.R. Critchley, E. Cannillo, V. Tazzoli, Acta Cryst. B 33 (1977) 456;
(e) K. Severin, R. Bergs, W. Beck, Angewant. Chem. Intl. Edn 37 (1998) 1634;
(f) H. Dialer, S. Schumann, K. Polborn, W. Steglich, W. Beck, Eur. J. Inorg. Chem. (2001) 1675;
(g) A.A.H. van der Zeijden, G. van Koten, R.A. Nordemann, B. Kojic-Prodic, A.L. Spek, Organomet 7 (1988) 1957.
[3] (a) G. Vujevic, C. Janiak, Z. Anorg, Allg. Chem. 629 (2003) 2585;
(b) I.C. Tornieporth-Oetting, P.S. White, Organometallics 14 (1995) 1632;
(c) T.M. Klapötke, H. Köpf, I.C. Tornieporth-Oetting, P.S. White, Organomet 13 (1994) 3628;
(d) W. Petri, J. Meder, M. Girnth-Weller, K. Bartel, V. Bejenke, G. Hüttner, W. Beck, Chem. Ber. 115 (1982) 846;
(e) M. Maurus, B. Aechter, W. Hoffmüller, K. Polborn, W. Beck, Z. Anorg, Allg. Chem. 623 (1997) 299;
(f) R. Dreos, G. Nardin, L. Randaccio, P. Siega, G. Tauzher, Inorg. Chem. 43 (2004) 3433.
[4] (a) R. Krämer, M. Maurus, R. Bergs, K. Polborn, K. Sünkel, B. Wagner, W. Beck, Chem. Ber. 126 (1993) 1969;
(b) R. Bergs, K. Sünkel, W. Beck, Chem. Ber. 126 (1993) 2429;
(c) R. Krämer, K. Polborn, H. Wanjek, I. Zahn, W. Beck, Chem. Ber. 123 (1990) 767;
(d) H. Wanjek, U. Nagel, W. Beck, Chem. Ber. 121 (1988) 1021.
[5] (a) J. Meder, W. Petri, W. Beck, Chem. Ber. 117 (1984) 827;
(b) H-G. Fick, W. Beck, J. Organomet. Chem. 252 (1983) 83;
(c) W. Beck, H. Bissinger, M. Girnth-Weller, B. Purucker, G. Thiel, H. Zippel, H. Seidenberger, B. Wappes, H. Schönenberger, Chem. Ber. 115 (1982) 2256.
[6] (a) Z. Nagy-Magos, B. Heil, L. Marko, Trans. Met. Chem. 1 (1976) 215;
(b) Z. Nagy-Magos, P. Kvintovics, L. Marko, Trans. Met. Chem. 5 (1980) 186.
[7] (a) K. Severin, S. Mihan, W. Beck, Chem. Ber. 128 (1995) 1127;
(b) T. Hauck, K. Sünkel, W. Beck, Inorg. Chim. Acta 235 (1995) 391.

[8] (a) D.G.H. Hetterscheid, C. Hendriksen, W.I. Dzik, J.M.M. Smits, E.R.H. van Eck, A.E. Rowan, V. Busico, M. Vacatello, V. Van Axel Castelli, A. Segre, E. Jellema, T.G. Bloemberg, B. de Bruin, J. Am. Chem. Soc. 128 (2006) 9746;
(b) K. Ahlford, J. Ekström, A.B. Zaitsev, P. Ryberg, L. Eriksson, H. Adolfsson, Chem. Eur. J. 15 (2009) 11197.
[9] M. Enamullah, M. Hasegawa, T. Hoshi, J. Okubo, J. Bangladesh Chem. Soc. 18 (2005) 165.
[10] M. Enamullah, A. Sharmin, M. Hasegawa, T. Hoshi, A-C. Chamayou, C. Janiak, Eur. J. Inorg. Chem. (2006) 2146.
[11] (a) C. Janiak, A-C. Chamayou, A.K.M. Royhan Uddin, M. Uddin, K.S. Hagen, M. Enamullah, Dalton Trans. (2009) 3698;
(b) M. Enamullah, A.K.M. Royhan Uddin, M. Uddin, J. Bangladesh Chem. Soc. 21 (2008) 28.
[12] M. Enamullah, M. Uddin, W. Linert, J. Coord. Chem. 60 (2007) 2309.
[13] (a) S.-K. Leung, K.Y. Kwok, K.Y. Zhang, K.K.-W. Lo, Inorg. Chem. 49 (2010) 4984;
(b) K.K.-W. Lo, C.-K. Li, K.-W. Lau, N. Zhu, Dalton Trans. (2003) 4682;
(c) S. Sprouse, K.A. King, P.J. Spellane, R.J. Watts, J. Am. Chem. Soc. 106 (1984) 6647;
(d) D. Ramlot, M. Rebarz, L. Volker, M. Ovaere, D. Beljonne, W. Dehaen, L. Van Meervelt, C. Moucheron, A. Kirsch-De Mesmaeker, Eur. J. Inorg. Chem. (2013) 2031;
(e) L. Flamigni, B. Ventura, F. Barigelletti, E. Baranoff, J.-P. Collin, J.-P. Sauvage, Eur. J. Inorg. Chem. (2005) 1312.
[14] SMART, Data Collection Program for the CCD Area-detector System; SAINT, Data Reduction and Frame Integration Program for the CCD Area-detector System, Bruker Analytical X-ray Systems, Madison, Wisconsin, USA, 1997.
[15] G. Sheldrick, Program SADABS: Area-detector Absorption Correction, University of Göttingen, Germany, 1996.
[16] G.M. Sheldrick, SHELXS-97, SHELXL-97, Programs for Crystal Structure Analysis, University of Göttingen, Germany, 1997.
[17] DIAMOND 3.0e for Windows. Crystal Impact Gbr, Bonn, Germany; http://www.crystalimpact.com/diamond.
[18] H.D. Flack, Acta Crystallogr. A 39 (1983) 876.
[19] M.J. Frisch, G.W. Trucks, H.B. Schlegel, G.E. Scuseria, M.A. Robb, J.R. Cheeseman, G. Scalmani, V. Barone, B. Mennucci, G.A. Petersson, H. Nakatsuji, M. Caricato, X. Li, H.P. Hratchian, A.F. Izmaylov, J. Bloino, G. Zheng, J.L. Sonnenberg, M. Hada, M. Ehara, K. Toyota, R. Fukuda, J. Hasegawa, M. Ishida, T. Nakajima, Y. Honda, O. Kitao, H. Nakai, T. Vreven, J.A. Montgomery Jr., J.E. Peralta, F. Ogliaro, M. Bearpark, J.J. Heyd, E. Brothers, K.N. Kudin, V.N. Staroverov, R. Kobayashi, J. Normand, K. Raghavachari, A. Rendell, J.C. Burant, S.S. Iyengar, J. Tomasi, M. Cossi, N. Rega, J.M. Millam, M. Klene, J.E. Knox, J.B. Cross, V. Bakken, C. Adamo, J. Jaramillo, R. Gomperts, R.E. Stratmann, O. Yazyev, A.J. Austin, R. Cammi, C. Pomelli, J.W. Ochterski, R.L. Martin, K. Morokuma, V.G. Zakrzewski, G.A. Voth, P. Salvador, J.J. Dannenberg, S. Dapprich, A.D. Daniels, Ö. Farkas, J.B. Foresman, J.V. Ortiz, J. Cioslowski, D.J. Fox, Gaussian 09, Revision D.01, Gaussian, Inc., Wallingford CT, 2009.
[20] (a) A.D. Becke, Phys. Rev. A 38 (1988) 3098;
(b) C. Lee, W. Yang, R.G. Parr, Phys. Rev. B 37 (1988) 785;
(c) D. Andrae, U. Häußermann, M. Dolg, H. Stoll, H. Preuß, Theor. Chim. Acta 77 (1990) 123;
(d) T.H. Dunning, J. Chem. Phys. 90 (1989) 1007;
(e) J.A. Fuentes, P. Wawrzyniak, G.J. Roff, M. Bühl, M.L. Clarke, Cat. Sci. Technol 1 (2011) 431;
(f) M.W. George, M.B. Hall, O.S. Jina, P. Portius, X.-Z. Sun, M. Towrie, H. Wu, X. Yang, S.D. Zarić, Proceed. Natl. Acad. Sci. 107 (2010) 20178;
(g) S. Bontemps, M. Sircoglou, G. Bouhadir, H. Puschmann, J.A. Howard, P.W. Dyer, K. Miqueu, D. Bourissou, Chem. A Eur. J. 14 (2008) 731.
[21] (a) E. Gross, W. Kohn, Adv. Quant. Chem. 21 (1990) 255;
(b) M. Marques, E. Gross, Annu. Rev. Phys. Chem. 55 (2004) 427;
(c) S. Miertuš, E. Scrocco, J. Tomasi, Chem. Phys. 55 (1981) 117;
(d) J. Tomasi, B. Mennucci, R. Cammi, Chem. Rev. 105 (2005) 2999;
(e) S. Miertus, J. Tomasi, Chem. Phys. 65 (1982) 239.
[22] (a) M.D. Ward, Chem. Commun. 47 (2005) 5838;
(b) F. Zhuge, B. Wu, J. Liang, J. Yang, Y. Liu, C. Jia, C. Janiak, N. Tang, X.J. Yang, Inorg. Chem. 48 (2009) 10249;
(c) B. Gil-Hernández, J.K. Maclaren, H.A. Höppe, J. Pasan, J. Sanchiz, C. Janiak, CrystEngComm 14 (2012) 2635;
(d) J.K. Maclaren, C. Janiak, Inorg. Chim. Acta 389 (2012) 183;
(e) D. Mekhatria, S. Rigolet, C. Janiak, A. Simon-Masseron, M. Abdelkrim Hasnaoui, A. Benguedach, Cryst. Growth Des. 11 (2011) 396;
(f) A.-C. Chamayou, M.A. Neelakantan, S. Thalamuthu, C. Janiak, Inorg. Chim. Acta 365 (2011) 447;
(g) B. Gil-Hernández, H. Höppe, J.K. Vieth, J. Sanchiz, C. Janiak, Chem. Commun. 46 (2010) 8270;
(h) G.R. Desiraju, T. Steiner, The Weak Hydrogen Bond, in: IUCr Monograph on Crystallography, vol. 9, Oxford Science, Oxford, 1999.
[23] (a) J.P. Merrick, D. Moran, L. Radom, J. Phys. Chem. A 111 (2007) 11683;
(b) M.A. Halim, D.M. Shaw, R.A. Poirier, J. Mol. Struct. THEOCHEM 960 (2010) 63;
(c) F.E. Jorge, J. Autschbach, T. Ziegler, Inorg. Chem. 42 (2003) 8902.
[24] M. Enamullah, M.A. Quddus, M.A. Halim, M.K. Islam, V. Vasylyeva, C. Janiak, Inorg. Chim. Acta 427 (2015) 103.
[25] M. Enamullah, A.K.M. Royhan Uddin, G. Pescitelli, R. Berardozzi, G. Makhloufi, V. Vasylyeva, A-C. Chamayou, C. Janiak, Dalton Trans. 43 (2014) 3313.
[26] (a) V. Gutmann, The Donor-Acceptor Approach to Molecular Interactions, Plenum Press, NY, 1978;
(b) M. Enamullah, F. Renz, U. El-Ayaan, G. Wiesinger, W. Linert, Vib. Spectros 14 (1997) 95;
(c) M. Enamullah, W. Linert, J. Coord, Chem. 40 (1996) 193.
[27] (a) M. Enamullah, M.K. Islam, J. Coord. Chem. 66 (2013) 4107;
(b) M. Enamullah, W. Linert, V. Gutmann, R.F. Jameson, Monatsh. für Chem. 125 (1994) 1301;
(c) M. Enamullah, W. Linert, V. Gutmann, Vib. Spectros 9 (1995) 265.
[28] (a) T. Akitsu, Y. Einaga, Polyhedron 24 (2005) 1869;
(b) T. Akitsu, Y. Einaga, Polyhedron 24 (2005) 2933;
(c) T. Akitsu, Polyhedron 26 (2007) 2527.
[29] (a) I. Veroni, A. Rontoyianni, C.A. Mitsopoulou, Dalton Trans. (2003) 255;
(b) M. Enamullah, J. Coord. Chem. 42 (1997) 231;
(c) W. Linert, M. Enamullah, V. Gutmann, R.F. Jameson, Monatsh. für Chem. 125 (1994) 661.
[30] (a) L. Dadci, H. Elias, U. Frey, A. Hornig, U. Kölle, A.E. Merbach, H. Paulustd, J.S. Schneider, Inorg. Chem. 34 (1995) 306;
(b) J.W. Bats, A.R. Nass, A.S.K. Hashmi, Acta Cryst. E60 (2004) m85;
(c) A. Boixassa, R. Mathieu, N. Lugan, J. Pons, J. Ros, Acta Cryst. E59 (2003) m658;
(d) U. Kölle, R. Görissen, T. Wagner, Eur. J. Inorg. Chem. 128 (1995) 911.
[31] M. Enamullah, A-C. Chamayou, C. Janiak, Z. Naturforsch 62b (2007) 807.
[32] M. Enamullah, A.K.M. Royhan Uddin, G. Hogarth, C. Janiak, Inorg. Chim. Acta 387 (2012) 173.
[33] (a) M. Enamullah, J. Coord. Chem. 64 (2011) 1608;
(b) M. Enamullah, A.K.M. Royhan Uddin, G. Hogarth, J. Coord. Chem. 65 (2012) 4263.
[34] (a) G.S. Rodman, K.R. Mann, Inorg. Chem. 27 (1988) 3338;
(b) J. Karas, G. Huttner, K. Heinze, P. Rutsh, L. Zsolnai, Eur. J. Inorg. Chem. (1999) 405.
[35] M. Enamullah, M.A. Quddus, M.R. Hasan, G. Pescitelli, R. Berardozzi, Guido J. Reiß, C. Janiak, Eur. J. Inorg. Chem. (2015) 2758.
[36] (a) M. Fatima, C.G. da Silva, A.M. Trzeciak, J.J. Ziolkowski, A.J.L. Pombeiro, J. Organomet. Chem. 620 (2001) 174;
(b) I. Kovacik, O. Gevert, H. Werner, M. Schmittel, R. Sollner, Inorg. Chim. Acta 275–276 (1998) 435.